

# A COMPARISON STUDY OF LOW-COST PERSONAL LASER SCANNING SYSTEMS FOR FOREST PLOT-LEVEL INVENTORIES

Xiaochen Wang, Haiyun Yao, Yangyang Ma, Xinlian Liang \*

State Key Laboratory of Information Engineering in Surveying, Mapping and Remote Sensing, Wuhan University, Luoyu Road, NO.129, Wuhan, China - (xchwang, yaohaiyun, MaYangyang, xinlian.liang)@whu.edu.cn

## Commission III, WG III/1

**KEY WORDS:** Forest Inventory, Plot Level, Hand-held LiDAR, Real Time.

### ABSTRACT:

Forest resource is an essential part of the environment, and can be used for carbon sink, soil conservation, windbreak and sand fixation, which is of great significance to maintaining the balance of ecologic and sustainable city development. Due to the complexity of wildwood, the approach of traditional forest inventory is difficult, low-efficiency, and labour-intensive. Thus, a handheld personal laser scanning (PLS<sub>hh</sub>) system is proposed in this paper. To solve the limitation of low-cost LiDAR's FoV, two LiDAR scanners (Ouster OS-1-128 and Hesai PandarXT-32) are integrated in our PLS<sub>hh</sub> system. The enhancement of our PLS<sub>hh</sub> have been demonstrated by the experiments in field forest plots. The comparison of trajectory and the comparison of point cloud have been conducted extensively. Experiment results show that the trajectory estimated by two scanners (Ouster and Hesai) has a strong consistency with using one scanner (Ouster), with standard deviation at sub-centimetres level. And the trajectory deviation between two scanners and UWB is ~15cm, which is consistent with the inherent positioning accuracy of UWB sensors. In addition, the point cloud data obtained by two scanners or one scanner have been quantitatively evaluated by the TLS (Leica RTC 360) muti-scan. The difference between tree height extracted from two scanners and TLS data was small, even at sub-meter level only. But the tree height extracted from one scanner is lower ~8m in comparison with TLS data, because of the limitation of vertical FoV. Therefore, the great potential of our PLS<sub>hh</sub> system with two scanners has been shown in the application of forest inventory.

### 1. INTRODUCTION

Light detection and ranging (LiDAR) collects three-dimensional (3-D) point clouds from the environment. For the study of forest ecosystems, the LiDAR sensors have been mounted on various platforms, such as spaceborne lidar (Simard et al., 2011), airborne laser scanning (ALS) (Wang et al., 2016), unmanned-borne laser scanning (ULS) (Lin et al., 2011), mobile laser scanning (MLS) (Liang et al., 2014) personal laser scanning (PLS) (Liang et al., 2015), and terrestrial laser scanning (TLS) (Lichti, 2002).

Among these, TLS has the highest geometric data quality among all platforms, and has experienced rapid development in the last two decades and has become popular in plot-level forest investigation and monitoring (Liang et al., 2022). However, its data collection efficiency is relatively low, mostly due to the setup of reference targets for registration purpose. In contrast, the lightweight handheld Personal Laser Scanning (PLS<sub>hh</sub>) systems significantly improve the efficiency in forest inventories (Balenović et al., 2021). For example, the rate of the tree detection using PLS<sub>hh</sub> was reported to be higher than 90% (Bauwens et al., 2016; Gollob et al., 2020); the extraction of tree position showed high consistency between PLS<sub>hh</sub> and TLS, with RMSE ranging from 2.1 cm to 3.9 cm (Ryding et al., 2015; Cabo et al., 2018); the tree height measurement has been demonstrated to be effective and reliable under easy forest conditions and in the leaf-off period (Jurjević et al., 2020).

Accurate point clouds have been widely used in 3D modelling, virtual reality, cultural heritage protection, and smart forest

inventory. Hence, building the complete point clouds of the environment is one of the main objects of our PLS<sub>hh</sub> system. Currently, most commercial devices are equipped with only one low-cost LiDAR sensor (Balenović et al., 2021), such as GeoSLAM ZEB Horizon, Leica BLK2GO, etc. The intrinsic problem of such a system is a small FoV (field of view). Consequently, it becomes challenging for a comprehensive forest digitization. A solution to solve the small FoV is to rotate the sensor, e.g., ZEB Horizon (FARO Technologies, Inc., Florida, USA), Stonex X120GO (Stonex Inc., Milan, Italy), and GS-100G (Geosun Navigation Inc., Wuhan, China), etc. However, such a system includes movable components, consequently resulting in higher costs and non-negligible motion distortions.

Alternatively, more than one LiDAR sensors can be integrated to form a group of sensors to enlarge the FoV, e.g., to capture larger data coverage that is beneficial for SLAM algorithm and to acquire treetops that are challenging to capture in a single static system.

A PLS<sub>hh</sub> system is proposed in this paper. The system has two low-cost scanners orientated in different directions. Thus, the system is capable to cover a wide FoV using a simple configuration. In addition, this paper compared the trajectories and point cloud data with references to validate the effectiveness and the potential of using low-cost PLS<sub>hh</sub> in forest inventories.

The rest of this paper is organized as follows: the hardware of the PLS<sub>hh</sub> and experiment setup are described in Section 2. The PLS<sub>hh</sub> was tested in two forest plots. Section 3 reported the reference of trajectory and point cloud data. The extensive

\* Corresponding author

comparison was analysed and discussed in Section 4. The conclusion and the discussion of future work was in section 5.

## 2. THE SYSTEM AND EXPERIMENT

### 2.1 Hardware and Platform Structure

A lightweight PLS<sub>hh</sub> system was designed in this paper. The PLS<sub>hh</sub> consists of five parts, including two Lidar sensors, i.e., OS-1-128 (Ouster Inc., San Francisco, USA) and PandarXT-32 (Hesai Technology Inc., Shanghai, China), an IMU, i.e., Xsens MTI-G-710 (Xsens Technologies B.V., Enschede, Netherlands), an Ultra Wide Band (UWB) receiver (NoopLoop Technology Co., Ltd, Shenzhen, China), and an onboard computing unit, i.e., Intel NUC computer (Intel Corporation, California, USA), as shown in Figure 1. The specifications of two LiDARs are shown in Table 1.

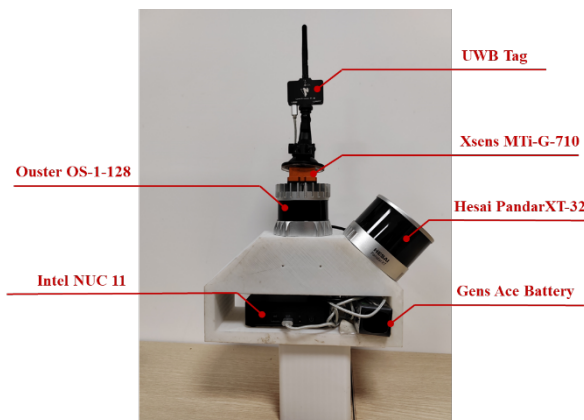


**Figure 1.** The experiment hardware structure.

Parameters	PandarXT-32	OS-1-128
Channel	32	128
FoV (Horizontal)	360°	360°
FoV (Vertical)	31°	45°
Range Capability	0.05 ~ 120 m	0.3 ~ 120 m
Range Precision	0.5 cm (typical)	±0.5 ~ ±3 cm
Wavelength	905 nm	865 nm
Weight	0.8 kg	0.42 kg (min)

**Table 1.** Specifications of PandarXT-32 and OS-1-128.

In this study, two LiDAR sensors were setup in the PLS<sub>hh</sub> system to enlarge the FoV, which are able to capture the data both horizontally and obliquely.

### 2.2 Extrinsic Calibration for Sensors

In order to build a joint point cloud from two individual data sets in the local coordinate systems, the LiDAR sensors were first calibrated. The extrinsic matrix between two scanners was calculated by selecting corresponding points manually, and refined by the ICP algorithm (Besl and Mckay, 1992). As shown in Figure 2, the point clouds captured from two scanners are coloured red and green respectively. The original data were in the coordinate system of themselves. After calibration, all points are transformed into a unified coordinate system.

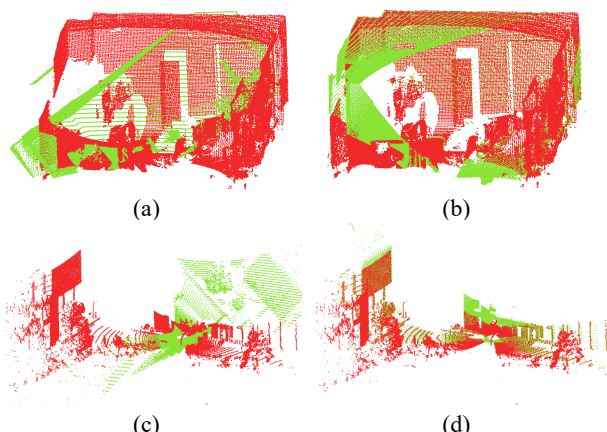


**Figure 2.** Extrinsic calibration between LiDAR sensors. (a), (b) The original and calibrated point clouds of indoor. (c), (d) The original and calibrated point clouds of outdoor.

In addition, the calibration between LiDARs and IMU was calculated by LI\_Init (Zhu et al., 2022). Finally, in order to compare the trajectories estimated by the UWB and the Lidar system, they are aligned by finding the rigid-body transformation corresponding to the least-squares solution (Horn, 1987).

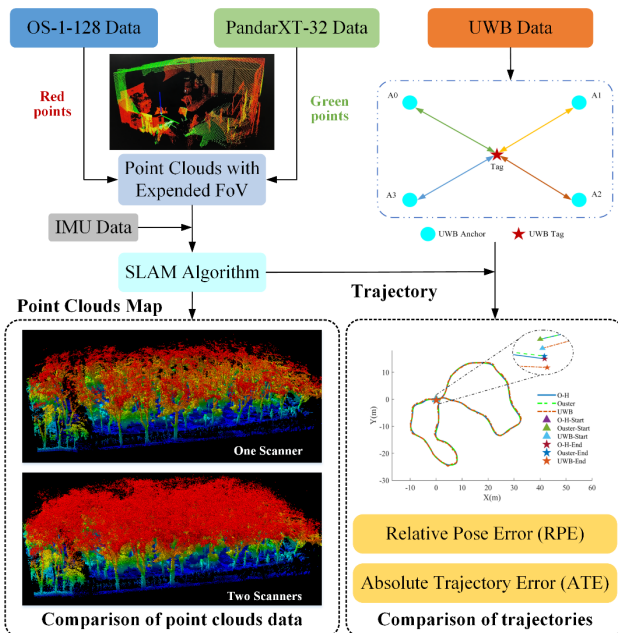
### 2.3 Study Area and Experiment Setup

The study area was located at Wuhan University (30.53°N, 114.36°E), Hubei Province, China. Two rectangular forest plots, approximately 40 m × 60 m, were utilized in this study. As shown in Figure 3, the dominant tree species in the study area is Cinnamomum Camphora.



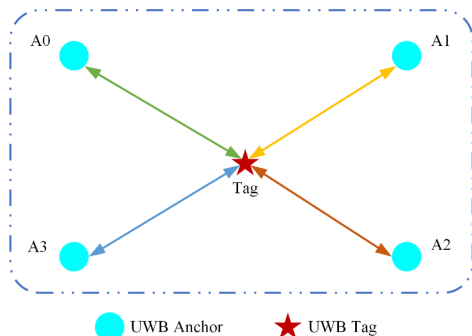
**Figure 3.** The study area

Figure 4 illustrated the experiment setup. At first, the point clouds from two scanners were calibrated and transferred in a unified coordinate. Then, the calibrated point clouds and motion data were fed into an excellent simultaneous localization and mapping (SLAM) algorithm, LIO-SAM. And the trajectory of operator and the integral point clouds of environment were obtained by SLAM. Finally, the UWB data and TLS data were employed to evaluate the trajectory accuracy and the completeness of point clouds.



**Figure 4.** The overview of experiment setup.

As shown in Figure 5, four UWB anchors and one UWB tag were setup in the study area to collect the trajectory of operator. Different types of walking path in the forest plot, such as square, z-shaped, and 8-shaped path, were recorded to have a comprehensive comparison of SLAM estimated. The position in local coordinate was obtained by a set of UWB devices.



**Figure 5.** Positioning by UWB devices.

The high spatial resolution and high range accuracy ( $1\text{mm}+10\text{ppm}$ ) TLS data were captured in the forest plots by the Leica RTC360 3D laser scanner (Leica Geosystems AG - Part of Hexagon, Heerbrugg, Switzerland), as shown in Figure 6. One central scan and four corner scans are made inside the forest plot to collect point clouds representing all trees within the plot, and these scans are accurately co-registered by using artificial reference targets manually placed throughout the plot.



**Figure 6.** The point cloud obtained by Leica RTC 360.

### 3. METHODOLOGY

#### 3.1 SLAM Algorithm

The LiDAR-based SLAM algorithm is able to derive user trajectories and 3D point clouds of environment in real-time in GNSS-denied environments, e.g., forest, mine, urban canyons, etc. Many excellent methods have been proposed for 3D LiDAR-based SLAM, such as LOAM (Zhang and Singh, 2014), LeGO-LOAM (Shan and Englot, 2018), and LIO-SAM (Shan et al., 2020). The LIO-SAM is a framework for tightly coupled lidar inertial odometry. It has been demonstrated that LIO-SAM can achieve the best accuracy when compared with LOAM, LeGO-LOAM, SC-LeGO-LOAM (Kim and Kim, 2018) and F-LOAM (Wang et al., 2021), in a variety of environments (Xu et al., 2022). Hence, the LIO-SAM algorithm is employed. For the detail of LIO-SAM, please refer to the paper (Shan et al., 2020).

#### 3.2 Trajectory Reference

An absolute positioning solution, UWB, with  $\sim 15$  cm positioning accuracy (Yao et al., 2022), was adopted to compare the trajectory of our PLS<sub>hh</sub> system.

The distance between UWB anchors and tag can be calculated by the Time of Flight (TOF), time of arrival (TOA), and time difference of arrival (TDOA), according to (Sahinoglu et al., 2008). Since the TOF method does not require the time synchronization between UWB anchors and tags, it is selected in this experiment. After that, in Figure 5, the UWB tag position  $(X_{tag}, Y_{tag}, Z_{tag})$  can be calculated by solving equation (1).

$$\begin{cases} (X_{tag} - X_{A1})^2 + (Y_{tag} - Y_{A1})^2 + (Z_{tag} - Z_{A1})^2 = d_1^2 \\ (X_{tag} - X_{A2})^2 + (Y_{tag} - Y_{A2})^2 + (Z_{tag} - Z_{A2})^2 = d_2^2 \\ \vdots \\ (X_{tag} - X_{An})^2 + (Y_{tag} - Y_{An})^2 + (Z_{tag} - Z_{An})^2 = d_n^2 \end{cases} \quad (1)$$

where  $(X_{tag}, Y_{tag}, Z_{tag})$  = the position of UWB tag  
 $(X_{A1}, Y_{A1}, Z_{A1}) \dots (X_{An}, Y_{An}, Z_{An})$  = the position of UWB anchors.  
 $d_1, d_2 \dots d_n$  = the distance between UWB tag and each anchor.

#### 3.3 Trajectory Evaluation

The statistics of Relative Pose Error (RPE) and Absolute Trajectory Error (ATE) (Sturm et al., 2012) were used to evaluate the difference between trajectories estimated by one scanner (Ouster alone), two scanners (Ouster and Hesai), and the UWB.

The RPE measures the local difference between the trajectories over a fixed time interval  $\Delta$ . The RPE at time step  $i$  was defined as equation (2).

$$E_i = (Q_i^{-1} Q_{i+\Delta})^{-1} (P_i^{-1} P_{i+\Delta}). \quad (2)$$

where  $E_i$  = the RPE value at time step  $i$   
 $\Delta$  = the fixed time interval  
 $Q_i, Q_{i+\Delta}$  = the poses of reference trajectory at time step  $i$  and time step  $i + \Delta$   
 $P_i, P_{i+\Delta}$  = the poses of the trajectory to be evaluated at time step  $i$  and time step  $i + \Delta$

The global consistency of the estimated trajectory was evaluated by calculating the absolute distances between different trajectories. Similar to RPE, the ATE at time step  $i$  can be defined as equation (3).

$$F_i = Q_i^{-1} S P_i. \quad (3)$$

where  $F_i$  = the ATE value at time step  $i$   
 $S$  = the transformation matrix between two trajectories  
 $Q_i$  = the pose of reference trajectory at time step  $i$   
 $P_i$  = the pose of the trajectory to be evaluated at time step  $i$

Based on the RPE and ATE, the common statistics, such as Maximum, Minimum, Mean, Median, and Standard Deviation, were used to quantitatively compare different trajectories.

### 3.4 Point Cloud Reference and Evaluation

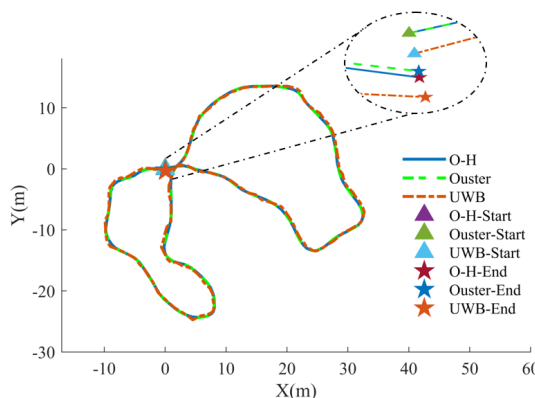
It is difficult to quantitative evaluation of the quality of point cloud data. In this paper, the point clouds data collected by TLS was employed as the ground truth. And then, the tree height, an

essential tree attribute, was utilized as the evaluation metric of completeness. The statistics of tree heights, i.e., Minimum, Maximum, Mean, and Median values, are summarized to have a quantitative comparison of different point clouds.

## 4. RESULTS AND DISCUSSION

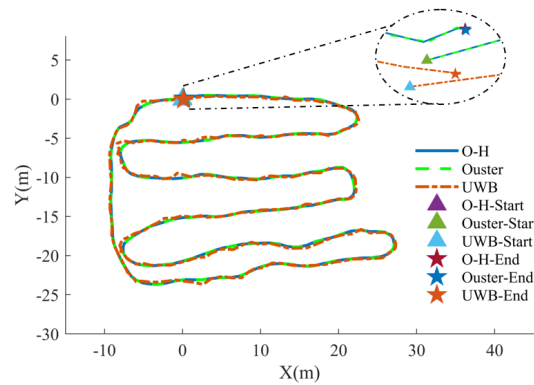
### 4.1 Trajectory Estimation and Comparison

The comparison of different trajectories was considered, including estimated by two scanners, estimated by one scanner, and UWB measured. As shown in Figure 7 and Figure 8, all the trajectories were plotted together for visual comparison. The blue solid line, green dashed line, and orange dash-dotted line represent the trajectory estimated by two scanners, one scanner, and UWB devices respectively. The upward-pointing triangles in purple, green, and blue represent the starting points of three types of trajectory, respectively. The pentagrams with colours red, blue, and orange, represent the ending points of three types of trajectory respectively. The ellipse area zooms in on the location of the start and end points, making it easier to read.



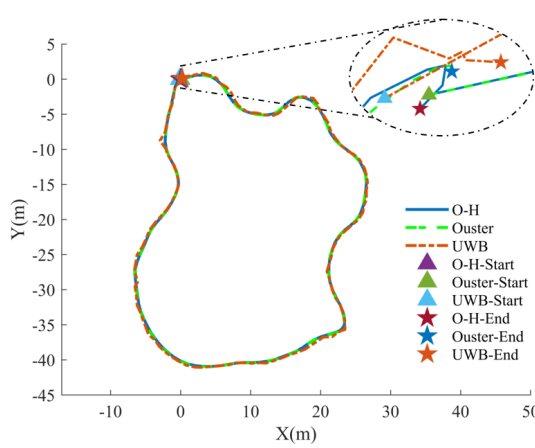
(a)

Figure 7. The trajectories of different walking paths in Plot-1. (a) The 8-shaped path.



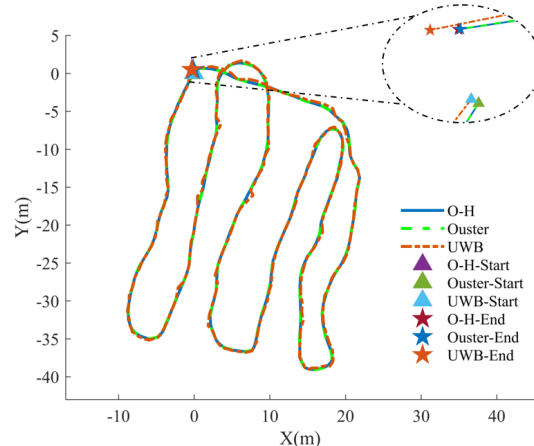
(b)

Figure 7. The trajectories of different walking paths in Plot-1. (b) The Z-shaped path



(a)

Figure 8. The trajectories of different walking paths in Plot-2. (a) The Square-shaped path.



(b)

Figure 8. The trajectories of different walking paths in Plot-2. (b) The Z-shaped path.

From the visualization of trajectory plotted in Figure 7 and Figure 8, it can be found that different trajectories were close to each other. All the starting points and ending points of them nearly overlap. But there are some mutations in the UWB trajectory, because of its inherent positioning errors and the NLOS impacts.

Overall, the three types of trajectories corroborate each other and validate the effectiveness of our PLS<sub>hh</sub> system.

The statistics of RPE between two scanners, one scanner and UWB devices were summarized in Table 2, Table 3. It can be found that the trajectories estimated by two scanners and one

scanner have a strong consistency, with a standard deviation of sub-centimetres. And the comparison of two scanners and UWB is consistent with the accuracy level of existing results, with a maximum difference of ~1m and a standard deviation of ~15cm.

		Min (cm)	Max (cm)	Mean (cm)	Med (cm)	STD (cm)
Plot-1	8-shp	0.08	1.78	0.73	0.58	0.44
	Z	0.01	2.91	0.59	0.51	0.46
Plot-2	SQ	0.13	5.20	1.07	0.88	0.85
	Z	0.14	2.68	0.98	0.89	0.62

**Table 2.** The statistics of relative pose error (RPE) between two scanners and one scanner.

		Min (cm)	Max (cm)	Mean (cm)	Med (cm)	STD (cm)
Plot-1	8-shp	1.45	72.07	18.40	15.31	13.79
	Z	0.40	98.26	20.08	16.07	15.11
Plot-2	SQ	1.70	79.17	20.50	16.51	15.76
	Z	0.50	104.70	16.35	11.49	15.18

**Table 3.** The statistics of relative pose error (RPE) between two scanners and UWB devices.

Similarly, the statistics of ATE between two scanners and one scanner or UWB devices were summarized in Table 4, Table 5.

		Min (cm)	Max (cm)	Mean (cm)	Med (cm)	STD (cm)
Plot-1	8-shp	0.01	4.19	1.42	1.23	0.78
	Z	0.00	3.43	1.42	1.43	0.66
Plot-2	SQ	0.01	8.49	3.62	3.44	1.93
	Z	0.00	3.48	1.17	1.05	0.71

**Table 4.** The statistics of absolute trajectory error (ATE) between two scanners and one scanner.

		Min (cm)	Max (cm)	Mean (cm)	Med (cm)	STD (cm)
Plot-1	8-shp	5.48	69.40	27.23	26.22	14.26
	Z	2.45	109.30	25.26	21.80	15.41
Plot-2	SQ	3.58	72.83	21.43	17.72	13.86
	Z	1.29	105.20	19.89	16.39	13.98

**Table 5.** The statistics of absolute trajectory error (ATE) between two scanners and UWB devices.

Similar to the results of RPE, the consistency of two scanners and one scanner also has been demonstrated by ATE. Besides, the ATE standard deviation of two scanners and UWB is also ~15cm.

#### 4.2 Point Clouds Mapping and Comparison

Figure 9 showed the point clouds obtained by one scanner, two scanners for a visual comparison.

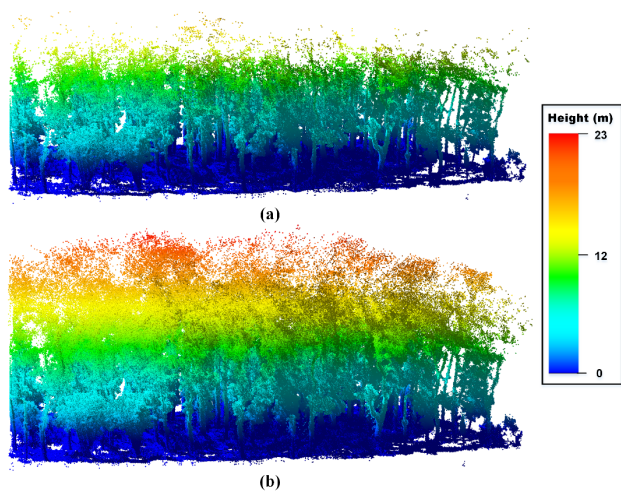


**Figure 9.** Examples of point clouds obtained by our PLS<sub>hh</sub> system. (a) One Scanner. (b) Two scanners

The point cloud in Figure 9 was rendered by height, and it should be mentioned that only the point cloud of forest plot-1 has been displayed.

As shown in Figure 9(a), the tree canopy collected by only one scanner is incomplete. In contrast, the point cloud data captured by two scanners were able to represent the trees in plot well, as shown in Figure 9(b). And, its crown shape is consistent with the TLS point cloud in Figure 6.

In addition, the individual trees captured by one scanner, two scanners, and TLS are shown in Figure 10 for a detailed comparison.

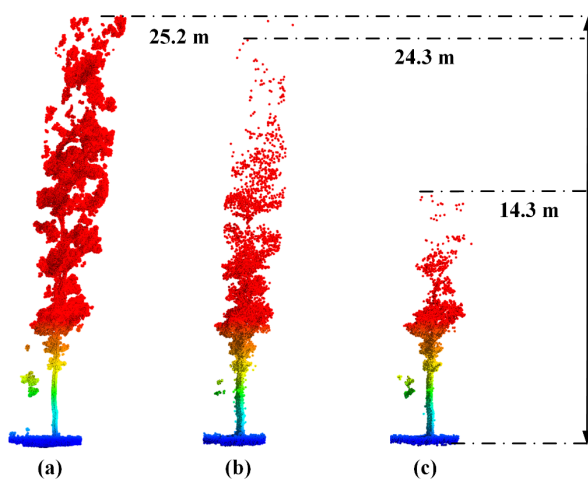


**Figure 10.** Examples of individual trees captured by different sensors. (a) TLS. (b) Two scanners. (c) One scanner.

In Figure 10, the point clouds of an individual tree captured by two scanners is more similar to TLS data in comparison with the one scanner setup. Although the data from two scanners is sparse, it significantly compensates for the missing point clouds obtained by one scanner. And the tree height values measured manually from TLS data, two scanners, and one scanner are 25.2m, 24.3m, and 14.3m respectively. All these demonstrate the enhancement made by setting up two scanners on our PLS<sub>hh</sub> system.

For a qualitative evaluation, the number of trees and the statistics of tree heights, i.e., Minimum, Maximum, Mean, and Median values, extracted from TLS data, two scanners, or one scanner are summarized in Table 6.

		Num. of Trees	Min (m)	Max (m)	Mean (m)	Med (m)
Plot-1	TLS	137	18.40	25.80	22.99	23.15
	Two scanners	166	15.78	25.12	21.72	22.17
	One scanner	173	9.81	18.32	14.23	14.11
Plot-2	TLS	139	14.40	23.79	20.84	21.29
	Two scanners	195	10.20	23.12	19.45	20.25
	One scanner	237	8.48	21.17	14.84	14.76

**Table 6.** The statistics of tree height were extracted from three types of point cloud data.

It can be found that the number of extracted trees has a large variation. Due to the lack of points at tree top, the canopy height model (CHM) is rough and difficult to detect individual trees accurately. Nevertheless, the result of two scanners is closer to TLS data in all forest plots. Furthermore, the tree height extracted from the point cloud captured by two scanners was closer to TLS data in comparison with the one scanner setup. In plot-1, the maximum tree height value extracted from two scanners is 0.68m lower, and the mean and median values are ~1m lower with the comparison of TLS data. But the statistics of tree height extracted from one scanner is lower ~8m with the comparison of TLS data, because of the limitation of vertical FoV. The similar performance is shown in plot-2.

For an intuitive representation, the tree height differences between TLS, two scanners, and one scanner are illustrated in Figure 11 and Figure 12. It indicates that the two-scanner setup further reduces the deviation of tree height in all metrics compared with the one scanner setup. Thus, the enhancement of FoV has been demonstrated in forests.

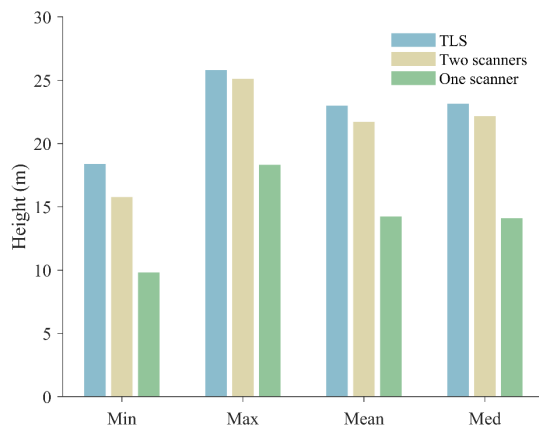


**Figure 11.** Different statistics of tree height in plot-1.

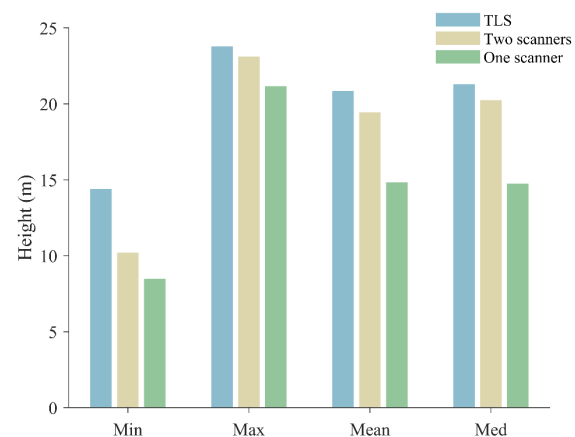


**Figure 12.** Different statistics of tree height in plot-2.

## 5. CONCLUSION

A new PLS<sub>hh</sub> system was presented in this study, and its effectiveness has been demonstrated by the comprehensive comparison of trajectory and point cloud. Firstly, the hardware structure of physical prototype was detailedly described, and the FoV was enlarged by setting two LiDAR scanners in complementary locations respectively. Then, the trajectories estimated by two scanners, one scanner, and UWB were compared qualitatively and quantitatively. Furthermore, the point cloud data collected by Leica RTC 360 were employed to be the ground truth. Based on this, the point cloud data obtained by two scanners or one scanner have been compared by the statistic of tree height.

The results from field experiment show that the trajectory of two scanners is strongly consistent with one scanner, with the standard deviation of RPE and ATE at sub-centimetres level. The comparison between the trajectory estimated by UWB devices set and two scanners is also consistent with its inherent positioning accuracy, with a maximum difference of ~1m and a standard deviation of ~15cm. For point clouds, the data obtained by two scanners is more complete than one scanner in visualization. Furthermore, it is also demonstrated by the tree height extracted from point clouds. The difference of tree height between two scanners and TLS data even at sub-meters. However, the tree height extracted from one scanner or TLS data has a ~8m difference, which is much larger than the deviation of tree height extracted from two scanners.

In general, our PLS<sub>hh</sub> system has been demonstrated to be a practical and convenient instrument in field forest inventory. The enhancement of PLS point cloud quality and the potential to extract more forest parameters will be further studied.

## ACKNOWLEDGEMENTS

This study was jointly supported by the Project of Background Resources Survey in Shennongjia National Park (SNJNP2023015), Open Project Fund of Hubei Provincial Key Laboratory for Conservation Biology of Shennongjia Snub-nosed Monkeys (SNJGKL2023015), Wuhan University (No. WHUZZJJ202220) and 2023 ISPRS Scientific Initiatives (Benchmarking of absolute and relative positioning solutions under GNSS denied environments for mobile geomatics).

## REFERENCES

- Balenović, I., Liang, X., Jurjević, L., Hyppä, J., Seletković, A., and Kukko, A., 2021: Hand-held personal laser scanning—current status and perspectives for forest inventory application, Croatian Journal of Forest Engineering: Journal for Theory and Application of Forestry Engineering, 42(1), 165-183.
- Bauwens, S., Bartholomeus, H., Calders, K., and Lejeune, P., 2016: Forest inventory with terrestrial LiDAR: A comparison of static and hand-held mobile laser scanning: *Forests*, 7, 127.
- Besl, P. J. and McKay, N. D., 1992: A method for registration of 3-D shapes: *IEEE Transactions on Pattern Analysis and Machine Intelligence*, 14(2), 239-256.
- Cabo, C., Del Pozo, S., Rodríguez-Gonzálvez, P., Ordóñez, C., and González-Aguilera, D., 2018: Comparing terrestrial laser scanning (TLS) and wearable laser scanning (WLS) for individual tree modeling at plot level: *Remote Sensing*, 10, 540.
- Gollob, C., Ritter, T., and Nothdurft, A., 2020: Forest inventory with long range and high-speed personal laser scanning (PLS) and simultaneous localization and mapping (SLAM) technology, *Remote Sensing*, 12, 1509.
- Horn, B. K., 1987: Closed-form solution of absolute orientation using unit quaternions, *Josa a*, 4, 629-642.
- Jurjević, L., Liang, X., Gašparović, M., and Balenović, I., 2020: Is field-measured tree height as reliable as believed – Part II, A comparison study of tree height estimates from conventional field measurement and low-cost close-range remote sensing in a deciduous forest, *ISPRS Journal of Photogrammetry and Remote Sensing*, 169, 227-241.
- Kim, G. and Kim, A., 2018: Scan Context: Egocentric Spatial Descriptor for Place Recognition Within 3D Point Cloud Map, 2018 IEEE/RSJ International Conference on Intelligent Robots and Systems (IROS), 1-5 Oct. 2018, 4802-4809, doi.org/10.1109/IROS.2018.8593953.
- Liang, X., Hyppä, J., Kukko, A., Kaartinen, H., Jaakkola, A., and Yu, X., 2014: The Use of a Mobile Laser Scanning System for Mapping Large Forest Plots, *IEEE Geoscience and Remote Sensing Letters*, 11(9), 1504-1508.
- Liang, X., Wang, Y., Jaakkola, A., Kukko, A., Kaartinen, H., Hyppä, J., Honkavaara, E., and Liu, J., 2015: Forest Data Collection Using Terrestrial Image-Based Point Clouds From a Handheld Camera Compared to Terrestrial and Personal Laser Scanning, *IEEE Transactions on Geoscience and Remote Sensing*, 53(9), 5117-5132.
- Liang, X., Kukko, A., Balenović, I., Saarinen, N., Junntila, S., Kankare, V., Holopainen, M., Mokroš, M., Surový, P., Kaartinen, H., Jurjević, L., Honkavaara, E., Näsi, R., Liu, J., Hollaus, M., Tian, J., Yu, X., Pan, J., Cai, S., Virtanen, J. P., Wang, Y., and Hyppä, J., 2022: Close-Range Remote Sensing of Forests: The state of the art, challenges, and opportunities for systems and data acquisitions, *IEEE Geoscience and Remote Sensing Magazine*, 10(3), 32-71.
- Lichti, D. D., 2002: Ground-based laser scanners: operation, systems and applications, *Geomatica*, 56(1), 21-33.
- Lin, Y., Hyppä, J., and Jaakkola, A., 2011: Mini-UAV-Borne LIDAR for Fine-Scale Mapping, *IEEE Geoscience and Remote Sensing Letters*, 8(3), 426-430.
- Ryding, J., Williams, E., Smith, M. J., and Eichhorn, M. P., 2015: Assessing handheld mobile laser scanners for forest surveys, *Remote Sensing*, 7, 1095-1111.
- Sahinoglu, Z., Gezici, S., and Güvenc, I., 2008: Ultra-wideband Positioning Systems: Theoretical Limits, Ranging Algorithms, and Protocols, Cambridge University Press, Cambridge.
- Shan, T. and Englot, B.: LeGO-LOAM: Lightweight and Ground-Optimized Lidar Odometry and Mapping on Variable Terrain, 2018 IEEE/RSJ International Conference on Intelligent Robots and Systems (IROS), 1-5 Oct. 2018, 4758-4765, 10.1109/IROS.2018.8594299.
- Shan, T., Englot, B., Meyers, D., Wang, W., Ratti, C., and Rus, D., 2020: LIO-SAM: Tightly-coupled Lidar Inertial Odometry via Smoothing and Mapping, *IEEE/RSJ International Conference on Intelligent Robots and Systems (IROS)*, 24 Oct.-24 Jan. 2021, 5135-5142, doi.org/10.1109/IROS45743.2020.9341176.
- Simard, M., Pinto, N., Fisher, J. B., and Baccini, A., 2011: Mapping forest canopy height globally with spaceborne lidar, *Journal of Geophysical Research: Biogeosciences*, 116(G4).
- Sturm, J., Engelhard, N., Endres, F., Burgard, W., and Cremers, D., 2012: A benchmark for the evaluation of RGB-D SLAM systems, *IEEE/RSJ international conference on intelligent robots and systems (IROS)*, 07-12 October 2012, 573-580, doi.org/10.1109/IROS.2012.6385773.
- Wang, H., Wang, C., Chen, C.-L., and Xie, L., 2021: F-LOAM : Fast LiDAR Odometry and Mapping, *IEEE/RSJ International Conference on Intelligent Robots and Systems (IROS)*, 27 Sept. 2021, doi.org/10.1109/iros51168.2021.9636655.
- Wang, Y., Hyppä, J., Liang, X., Kaartinen, H., Yu, X., Lindberg, E., Holmgren, J., Qin, Y., Mallet, C., Ferraz, A., Torabzadeh, H., Morsdorf, F., Zhu, L., Liu, J., and Alho, P., 2016: International Benchmarking of the Individual Tree Detection Methods for Modeling 3-D Canopy Structure for Silviculture and Forest Ecology Using Airborne Laser Scanning, *IEEE Transactions on Geoscience and Remote Sensing*, 54(9), 5011-5027.
- Xu, X., Zhang, L., Yang, J., Cao, C., Wang, W., Ran, Y., Tan, Z., and Luo, M., 2022: A Review of Multi-Sensor Fusion SLAM Systems Based on 3D LIDAR, *Remote Sensing*, 14, 2835.
- Yao, H., Wang, X., Qi, H., and Liang, X., 2022: TIGHTLY COUPLED INDOOR POSITIONING USING UWB/MMWAVE RADAR/IMU, *Int. Arch. Photogramm. Remote Sens. Spatial Inf. Sci.*, XLVI-3/W1-2022, 323-329, 10.5194/isprs-archives-XLVI-3-W1-2022-323-2022.
- Zhang, J. and Singh, S.: LOAM: Lidar odometry and mapping in real-time, *Robotics: Science and Systems*, 1-9.
- Zhu, F., Ren, Y., and Zhang, F., 2022: Robust real-time lidar-inertial initialization, *IEEE/RSJ International Conference on Intelligent Robots and Systems (IROS)*, 23-27 October 2022, 3948-3955, doi.org/10.1109/IROS47612.2022.9982225.